Reac Kinet Mech Cat (2016) 119:445–455
DOI 10.1007/s11144-016-1066-x

Structural and microstructural analysis of different CaO–NiO composites and their application as CO_2 or CO–O_2 captors

Alejandra Cruz-Hernández[1] · Brenda Alcántar-Vázquez[2] · Jesús Arenas[3] · Heriberto Pfeiffer[1]

Received: 23 May 2016 / Accepted: 11 August 2016 / Published online: 17 August 2016

Abstract In this work, CaO–NiO mixed oxide powders were prepared by mechanical mixing and incipient impregnation methods. The samples were characterized structurally and microstructurally, where it was determined that microstructural properties changed depending on the NiO addition method. The CO_2 and CO–O_2 capture evaluations were performed in a thermogravimetric analyzer. These results showed that the presence of nickel significantly modified the CO_2 and CO capture processes. In both cases, the CO_2 or CO capture temperature was shifted to lower values in the CaO–NiO composites in comparison to the CaO sample. Nevertheless, the carbon oxide captures seemed to decrease as a function of the nickel addition. It was associated to the nickel superficial deposition over the CaO particles. On the other hand, the CO–O_2 oxidation was importantly enhanced and maintained, for long times, with the presence of nickel independently of the calcium oxide carbonation process.

Keywords CO_2 capture · CO oxidation · Composites

Electronic supplementary material The online version of this article (doi:10.1007/s11144-016-1066-x) contains supplementary material, which is available to authorized users.

✉ Heriberto Pfeiffer
pfeiffer@iim.unam.mx

[1] Instituto de Investigaciones en Materiales, Universidad Nacional Autónoma de México, Circuito Exterior s/n, Ciudad Universitaria, Del. Coyoacán, 04510 Ciudad de México, Mexico

[2] Instituto de Ingeniería, Coordinación de Ingeniería Ambiental, Universidad Nacional Autónoma de México, Circuito Escolar s/n, Ciudad Universitaria, Del. Coyoacán, 04510 Ciudad de México, Mexico

[3] Instituto de Física, Universidad Nacional Autónoma de México, Circuito de la Investigación Científica s/n, Ciudad Universitaria, Del. Coyoacán, 04510 Cuidad de México, Mexico

Introduction

CO_2 is one of the major greenhouse gases (GHG) that absorbs heat radiation from the surface of Earth, which would otherwise leave the atmosphere [1]. Therefore, in recent years, the impact of global warming has been of particular concern worldwide [2–4]. Based on that, there are three challenges regarding environmental and energy issues: (1) finding a viable alternative energy source as a replacement for oil, (2) reducing CO_2 emissions and (3) preventing air pollution.

Within this context, reliable solid sorbent materials may be of great importance for carbon capture and sequestration. CO_2-sorbents, such as CaO and MgO, [1, 5, 6] have been intensively studied. In general, any metal oxide that would qualify for CO_2 capture applications must be abundant in the earth's crust, react with CO_2, allow regeneration, have suitable reaction kinetics, and form a carbonate stable in the environment at ambient conditions [5, 7–9]. CaO-based sorbents can be significantly improved by physical or chemical modifications [1]. Although numerous studies can be found in the literature about the carbonation, diffusion, structure, surface and reaction kinetics of CaO-based sorbents [10], considerably less information is available on CaO–NiO sorbents for CO_2 capture [11–13]. Choudhary et al. [14] found that a CaO–NiO composite can be used in the oxidative conversion of methane to syngas (H_2–CO). According to these authors, the highest conversion, selectivity and productivity occur far away from the reaction equilibrium. Moreover, at atmospheric pressure, practical CaO carbonation occurs in a narrow temperature window of 650–700 °C. At lower temperatures, the reaction rate is too slow for practical use [15, 16]. Recently, CO_2 capture in CaO–NiO was studied by Lee [17], where this composite was able to trap CO_2 at a lower temperature (465 °C) than pure calcium oxide. Therefore, in a first approach, the properties of CaO–NiO are worth studying in the production of syngas by CO_2 and steam-reforming reactions and CO_2 capture. CaO-based sorbents, obtained using different synthesis methods [13, 18–21] and exhibiting varying morphologies [22–24] and surface modifications [25], are also of special relevance in gas capture and heterogeneous catalysis.

There are few works related to the CO oxidation [26–30] and subsequent CO_2 capture in inorganic oxides. Therefore, the aim of this work is to elucidate the CO_2 capture and CO oxidation and subsequent CO_2 capture using CaO and different CaO–NiO systems prepared by metal oxide mixing and impregnation methods, analyzing the structural and microstructural characteristics of the CaO–NiO systems.

Experimental section

Initially, CaO and NiO were obtained by calcining $CaCO_3$ (Meyer 99.9 %) and $Ni(CH_3COO)_2$ (Sigma-Aldrich 99 %) at 900 and 600 °C for 6 h. Then, a composite was prepared by mixing both oxides in a molar ratio of CaO:NiO = 0.97:0.03 (labeled as CaO–NiO). The Ni-impregnated CaO sample was prepared as follows.

0.4 g of CaO, previously prepared as described above, was impregnated with 1100 μL of aqueous nickel solution (1 M nickel(II) nitrate hexahydrate, $Ni(NO_3)_2 \cdot 6H_2O$, Sigma-Aldrich 99 %) drop by drop. After that the sample was dried at room temperature and then it was calcined at 600 °C for 4 h (heating rate of 5 °C/min). It must be pointed out that these preparation methods were selected to evidence the importance of the NiO microstructural characteristics.

These samples were structurally and microstructurally characterized. The structural characterization was done with X-ray powder diffraction (XRD) using a Siemens D5000 diffractometer (CO_2 1.7903 Å radiation). The specific surface areas of the samples were calculated from N_2 adsorption–desorption isotherms using BEL-Japan MINI-sorp equipment at 77 K. The specific values of the surface areas were determined using the BET method. The powder morphology was observed and studied through SEM–EDS analysis in a JEOL JSM7800FEG scanning electron microscope. The particle sizes were determined by statistical standard method, measuring the particles in different images. For nanoparticle identification, HRTEM investigations were conducted on a JEOL JEM2010FEG transmission electron microscope. To quantify the calcium and nickel contents, a Varian SpectraAA 220 atomic absorption spectrometer was used.

Temperature-programmed CO_2 and CO desorption (TPD) experiments were performed on a BELCAT catalyst analyzer (BEL-Japan). Prior to the analysis, the samples were pretreated at 850 °C for 85 min under flowing He (30 mL/min) to remove any moisture and adsorbed impurities. After the catalyst activation, the sample was cooled to 40 °C. Then, carbon dioxide or carbon monoxide was fed into the equipment using a gas flow of 50 mL/min for 60 min. Finally, the sample was heated in a He flow at a rate of 10 °C/min from 40 to 850 °C, measuring the thermal conductivity changes associated with the sorbed CO_2 or CO molecules.

CO_2 and CO–O_2 capture experiments were performed in a TA Instruments Q-500HR thermobalance by varying the temperature from 30 to 850 °C. The CO–O_2 catalytic reaction was analyzed using a catalytic reactor with a gas mixture of 5 vol% O_2 (Praxair, grade 2.6), 5 vol% CO, and balance N_2 (Praxair, certified mixture) with a total flow rate of 100 mL/min. Each sample was heated from 30 to 900 °C at a rate of 5 °C/min. The gas products were analyzed in a GC 2014 gas chromatograph (Shimadzu) with a Carboxen-1000 column coupled with an Alpha Platinum FTIR (Bruker with a ZnS gas cell).

Results and discussion

As determined by X-ray diffraction, Fig. 1 shows the various crystalline compounds present in the powders obtained from the CaO synthesis and the different nickel additions (mechanically and by impregnation). In the CaO sample, only this compound was detected and fitted to the PDF 37-1497 file, as expected. In the CaO–NiO composite, part of the calcium oxide seemed to be hydrated, as small $CaO \cdot H_2O$ crystals (PDF file 02-0968) were present, and NiO was also obtained (PDF file 47-1049). The nickel addition and the mechanical process thereby induced a partial hydration of the main CaO phase. In the Ni-impregnated CaO sample, NiO was

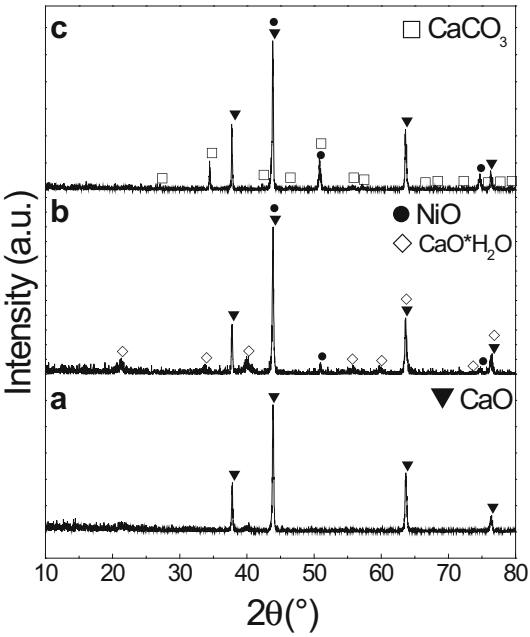

Fig. 1 XRD patterns of **a** CaO, **b** CaO–NiO composite and **c** Ni-impregnated CaO samples. Each compound present in the XRD patterns was labeled as CaO (*inverted filled triangle*), $CaO{\cdot}H_2O$ (*unfilled diamond*), NiO (*filled circle*) and $CaCO_3$ (*open square*)

detected, and part of the calcium was converted to $CaCO_3$ (PDF file 05-0586). This must be produced during the second heating process, where the nickel nitrate was decomposed at 600 °C in air, a temperature at which CaO is very reactive to CO_2, due to the slow sample carbonation process at room temperature [15]. Based on the presence of secondary phases, the samples were always thermally cleaned before the CO_2 chemisorption processes. Additionally, based on these results, the coexistence of the CaO and NiO phases is clearly evident.

After the structural characterization, it was necessary to determine the real content of nickel in the Ni-impregnated CaO sample by atomic absorption. The result indicates that the Ca:Ni molar ratio was 0.98:0.03, which is similar and comparable with the mechanical composite (see experimental section).

All the samples were microstructurally analyzed by N_2 adsorption, scanning and transmission electron microscopies. All the samples presented N_2 adsorption–desorption isotherms type II isotherms, according to the IUPAC classification [31], corresponding to non-porous samples (see supplementary information). The specific surface areas determined by the BET model were 14, 12 and 8 m^2/g for the CaO, CaO-NiO and Ni-impregnated CaO samples. It is evident that the nickel addition tends to decrease the total surface area. It can be explained based in the fact that nickel oxide, in the composite sample, possesses a lower surface area (4.5 m^2/g), reducing the total sample surface. Simultaneously, in the Ni-impregnated CaO sample, nickel is deposited over the CaO surface, producing a surface area decrement but mainly the surface decrement may be associated to the second calcination process of this sample, which should have produced the sample sintering. In addition to the textural analysis performed by N_2 adsorption–

desorption, the microstructural analysis was complemented by scanning and transmission electron microscopies. Fig. 2 shows scanning electron images displaying the general morphology of the pristine CaO and the nickel-added samples. The pristine CaO showed well-defined micrometric cubes (2–10 m sides). These cubes seem to be composed of small sintered particles, which produce some form of macroporosity. The morphology of the CaO–NiO composite showed the presence of the same CaO micrometric cubes covered with many small polyhedral particles of approximately 200-300 nm. These tiny particles must correspond to the NiO located over the CaO particle surfaces. Finally, in the Ni-impregnated CaO sample, the surface morphology changed, as the CaO surface evidenced the deposition and incrustation of particles with two different sizes: 50–100 nm and approximately 1 m. Again, both types of particle must correspond to the nickel particles deposited after the impregnation and thermal processes. To further analyze the Ni-impregnated sample, a mapping elemental analysis was performed (Fig. 3). From this elemental analysis, it is evident that the deposited particles contain nickel and are most probably nickel oxide. As the smallest particles could not be analyzed by this technique, transmission electron microscopy images were obtained. Fig. 4 shows a HR-TEM image, where nanoparticles of approximately 2–3 nm could be indexed with the NiO cubic phase (Fm $\overline{3}$ m). Therefore, the nickel particles are

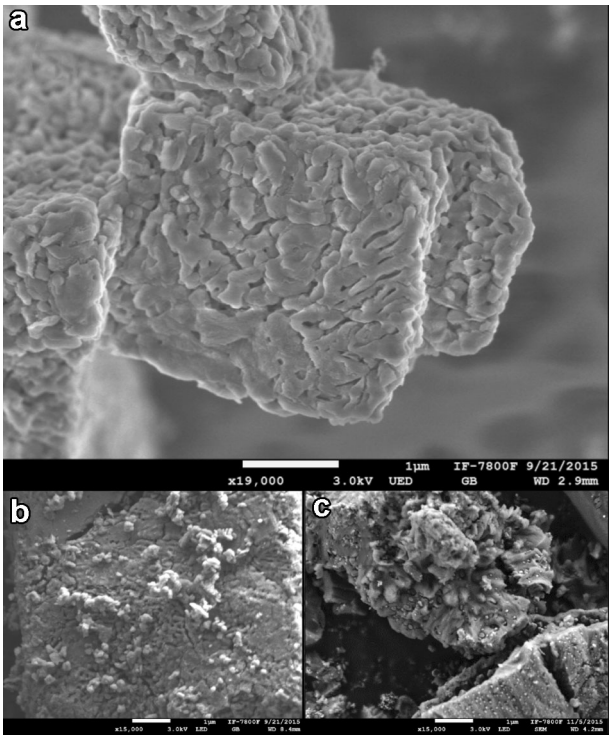

Fig. 2 Secondary electron images of **a** CaO, **b** CaO–NiO composite and **c** Ni-impregnated CaO samples. These images show that sample morphology changed depending on their preparation method

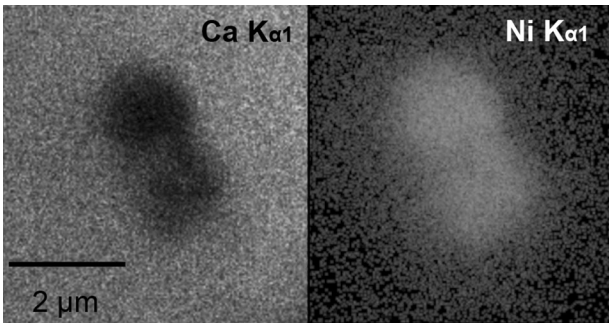

Fig. 3 Microscopic composed image of the elemental mapping distribution of Ca and Ni on the Ni-impregnated CaO sample. The *bright areas* indicate the presence of the corresponding element

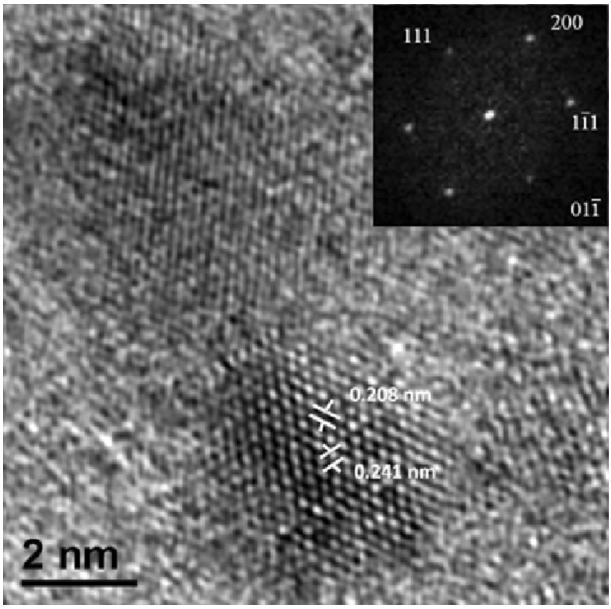

Fig. 4 HR-TEM image of Ni-impregnated CaO sample, where it was identified the NiO nanoparticle. The *square inset* show the electron diffraction pattern, which indexes in the $[01\bar{1}]$ direction

deposited over the CaO with significantly varying size, from micro- to nano-particles.

After the structural and microstructural studies, the temperature-programmed desorption experiments of CO_2 (CO_2-TPD) and CO (CO-TPD) were performed on the pristine and Ni-added CaO samples (see supplementary information). In the CO_2 case, there are three processes in all the samples. The pristine CaO sample presents three temperature regions for CO_2 desorption at 90, 310 and 560 °C, which must correspond to CO_2 adsorbed, superficially chemisorbed and chemisorbed in the CaO particle bulk. A comparison of the obtained temperature regions for CaO sample

revealed that these temperatures were in agreement for the first and third peaks, with literature [32–34]. Although two of the peaks evidenced in these experiments are in good agreement with the previous reports, the peak located at 310 °C was not fully identified. Nevertheless, this peak must correspond to a superficial carbonation process, as it is supported by the TG results presented below. The CO_2-TPD curves of the Ni-added samples present the same desorption peaks, but at lower temperatures, in both cases. Perhaps the most evident temperature shift corresponds to the bulk CO_2 chemisorption, as it was observed at 554 and 551 °C. This means that the CO_2 desorption was shifted to lower temperatures. These results suggest that the presence of Ni destabilizes the CO_2 carbonation-decarbonation process in CaO. On the other hand, when CO gas was used as an adsorbent, the samples presented important differences. The CaO sample showed only two peaks at approximately 337 °C (strong) and 500 °C (narrow), which may be associated with CO chemisorbed at the surface and in bulk CaO particles. However, when nickel was included in the CaO, as a composite or impregnated, the CO-TPD curves changed. In the CaO–NiO composite, two different peaks appeared at 285 and 360 °C. Therefore, the CO superficial chemisorption must be produced in both the CaO and NiO particles. However, the Ni-impregnated sample only showed one desorption peak at high temperature (680 °C), which may be attributed to CO_2. The formation of CO_2 could occur through the direct oxidation of adsorbed CO on the NiO nanoparticles. This result suggests CO oxidation and consequent carbonation, with the corresponding nickel oxide reduction, as it was confirmed below.

After the chemical, structural and microstructural characterizations, the CO_2 and CO–O_2 captures were evaluated in all the samples. Fig. 5 shows the dynamic TG experiments of the three CaO samples. Initially, for the CO_2 capture process (Fig. 5a), the pristine CaO presented a typical behavior, where two different processes are observed [12]. The first weight increment was depicted between 300 and 520 °C. This weight increment is associated with the superficial CO_2

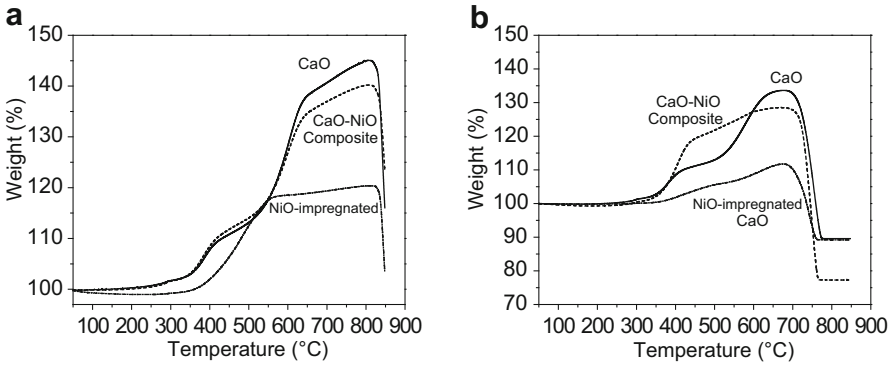

Fig. 5 Thermogravimetric dynamic curves of **a** CO_2 capture (from 30 to 850 °C at 5 °C/min, flowing 100 mL/min of CO_2) and **b** CO oxidation with subsequent CO_2 capture (from 30 to 850 °C at 5 °C/min, flowing 100 mL of a mixture of 5 vol% O_2 and 5 vol% CO N_2 balanced). Both experiments were performed in the CaO, CaO–NiO composite and Ni-impregnated CaO samples, where the presence of nickel into the samples decreased significantly the CO_2 capture temperature in both gas flows

chemisorption, where a $CaCO_3$ external shell is produced. Then, once the diffusion processes are activated and the CO_2 chemisorption can continue through the ceramic bulk, the second weight increment was observed (525–825 °C). Finally, at $T > 825$ °C, the $CaCO_3$ decomposition process occurs, as evidenced by a weight decrement. The CaO–NiO composite presents a very similar behavior to that previously described for the pristine CaO, with no real qualitative differences. However, the Ni-impregnated sample presents important differences. In this case, the superficial and bulk chemisorption processes were not different, and only one weight increment was depicted between 350 and 825 °C. Although these are qualitative experiments, the final weight increment was only half those observed in the previous samples. It seems that the Ni impregnation over the CaO surface particles inhibits the CO_2 capture process.

Fig. 5b shows the dynamic TG experiments of the three CaO samples using a $CO–O_2$ gas flow. As in the previous case, all these thermograms presented weight increments, confirming the carbon capture. The carbonation process in all the systems did not vary in temperature range in comparison to the CO_2 gas flow experiments; only the decarbonation process was shifted from 825 to 705 °C, which must be related to different equilibrium processes at the solid–gas interface due to the lower CO concentration. Moreover, the weight increments were lower, suggesting a slower kinetic process in comparison to the CO_2 results. Additionally, as in the previous case, the nickel oxide addition diminished the carbonation process. The carbonation processes, in the presence of CO_2 or $CO–O_2$, were confirmed qualitatively by ATR-FTIR, when the experiments were performed at different temperatures (data not shown).

At the same time, the CO catalytic conversion to CO_2 was evaluated in the samples. Fig. 6 shows the CO conversion and CO_2 formation as a function of temperature. CO conversion varied as a function of the composition. In fact, the 100 % CO conversion efficiency was shifted from 750 to 490 and 350 °C, using the

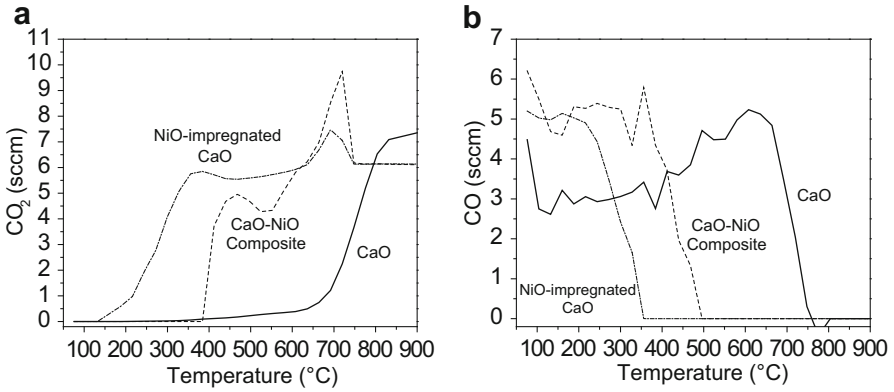

Fig. 6 Catalytic evolution of **a** CO_2 production and **b** CO conversion (determined by gas chromatography from 50 to 900 °C at 5 °C/min, flowing 100 mL of a mixture of 5 vol% O_2 and 5 vol% CO N_2 balanced) as a function of temperature, using CaO, CaO–NiO composite and Ni-impregnated CaO samples. The CO consumption fits well with the corresponding CO_2 production, as a function of temperature and nickel content

CaO, CaO–NiO composite and Ni-impregnated CaO samples. These temperature shifts must be associated to the fact that nickel is able to catalyze the CO oxidation process [35]. Moreover, pristine NiO presented a similar catalytic behavior than that observed on the Ni-impregnated CaO sample. Consequently, the CO_2 produced can be chemically trapped as soon as the CO is oxidized. Moreover, these CO conversion temperatures are in good agreement with the CO_2 production detected by the same experiments. In fact, the CaO–NiO composite and Ni-impregnated CaO samples presented higher CO_2 concentrations than that expected at approximately 680 °C, which must be associated with the $CaCO_3$ decarbonation that occurs in this temperature range. Hence, the quantified CO_2 corresponds to the catalytically converted CO and, at high temperatures, to the fraction of CO_2 previously converted and chemisorbed.

Conclusions

In this work, two different CaO–NiO composites were prepared, mechanically and by an incipient impregnation method. While the mechanical method simply produced a micrometric CaO and NiO mixture, the impregnation method allowed the production of NiO nanoparticles deposited on the CaO surface.

The CO_2 and CO–O_2 capture processes were performed in pristine CaO as well as in the CaO–NiO composites prepared mechanically and by impregnation. For the CO_2 capture, all the samples presented a typical behavior. Nevertheless, the CaO–NiO impregnated sample showed important differences in that the superficial and bulk chemisorption processes were the same, and only one slight weight increment was depicted. The differences observed were attributed to variations on the samples textural characteristics, but mainly to the nickel morphology. In the CO–O_2 case, the thermograms showed weight increments, as in the CO_2 case, confirming the carbon capture. These results were confirmed in a catalytic reactor, where the CO conversion to CO_2 was evaluated. It must be noted that in this case, the 100 % CO conversion efficiency was shifted from 750 to 490 and 350 °C using the CaO, CaO–NiO composite and Ni-impregnated CaO samples, showing the positive effect of the presence of nickel in this catalytic capture process. Therefore, although the CaO carbonation, in the presence of a CO–O_2 flow, was not the most efficient under these physicochemical conditions, the oxidation process was produced very actively from moderate to high temperatures.

Acknowledgments This work was financially supported by the project PAPIIT-UNAM (IN-101916) and SENER-CONACYT (251801). A. Cruz-Hernandez thanks to CONACYT for financial support. The authors thank to Adriana Tejeda, Roberto Hernández and Samuel Tehuacanero-Cuapa for technical help.

References

1. Wang J, Huang L, Yang R, Zhang Z, Wu J, Gao Y, Wang Q, O'Hare D, Zhong Z (2014) Recent advances in solid sorbents for CO_2 capture and new development trends. Energy Environ Sci 7:3478–3518
2. Cox P, Jones C (2008) Illuminating the modern dance of climate and CO_2. Science 321:1642–1644

3. Ahn J, Brook EJ (2008) Atmospheric CO_2 and climate on millennial time scales during the last glacial period. Science 322:83–85
4. Parry M, Canziani O, Palutikof J (2008) Key IPCC conclusions on climate change impacts and adaptations. World Meteorol Organ Bull 57(2):78–85
5. Kumar S, Saxena SK (2014) A comparative study of CO_2 sorption properties for different oxides. Mater Renew Sustain Energy 3:1–15
6. Abanades JC, Anthony EJ, Wang J, Oakey JE (2005) Fluidized bed combustion systems integrating CO_2 capture with CaO. Environ Sci Technol 39(8):2861–2866
7. Silaban A, Harrison DP (1995) High temperature capture of carbon dioxide: characteristics of the reversible reaction between CaO(s) and CO_2 (gas). Chem Eng Commun 137:177–190
8. Liu X, Piao X, Wang Y, Zhu S, He H (2008) Transesterification of soybean oil to biodiesel using CaO as a solid base catalyst. Fuel 87:216–221
9. Yan S, Lu H, Liang B (2008) Supported CaO catalysts used in the transesterification of rapeseed oil for the purpose of biodiesel production. Energy Fuels 22(1):646–651
10. Hughes R, Lu D, Anthony E, Wu Y (2004) Improved long-term conversion of limestone-derived sorbents for in situ capture of CO_2 in a fluidized bed combustor. Ind Eng Chem Res 43:5529–5539
11. Ring AT (1996) Fundamentals of Ceramic Powder Processing and Synthesis. Academic Press, New York
12. Mohammadi M, Lahijani P, Mohamed AR (2014) Refractory dopant-incorporated CaO from waste eggshell as sustainable sorbent for CO_2 capture: experimental and kinetic studies. Chem Eng J 243:455–464
13. Liu C, Zhang L, Deng J, Mu Q, Dai H, He H (2008) Surfactant-aided hydrothermal synthesis and carbon dioxide adsorption behavior of three-dimensionally mesoporous calcium oxide single-crystallites with tri-, tetra-, and hexagonal morphologies. J Phys Chem C 112:19248–19256
14. Choudhary VR, Rajput AM, Prabhakar B (1992) Low temperature oxidative conversion of methane to syngas over NiO–CaO catalyst. Catal Lett 15:363–370
15. Manovic V, Anthony EJ (2008) Thermal activation of CaO-based sorbent and self-reactivation during CO_2 capture looping cycles. Environ Sci Technol 42:4170–4174
16. Choudhary VR, Rajput AM (1996) Simultaneous carbon dioxide and steam reforming of methane to syngas over NiO-CaO catalyst. Ind Eng Chem Res 35:3934–3939
17. Lee ZH, Ichikawa S, Lee KT, Mohamed AR (2015) The role of nickel oxide additive in lowering the carbon dioxide sorption temperature of CaO. J Energy Chem 24:225–231
18. Samantaray S, Pradhan DK, Hota G, Mishra BG (2012) Catalytic application of CeO_2–CaO nanocomposite oxide synthesized using amorphous citrate process toward the aqueous phase one pot synthesis of 2-amino-2-chromenes. Chem Eng J 193–194:1–9
19. Gaki A, Chrysafi R, Kakali G (2007) Chemical synthesis of hydraulic calcium aluminate compounds using the Pechini technique. J Eur Ceram Soc 27:1781–1784
20. Mastin J, Aranda A, Meyer J (2011) New synthesis method for CaO-based synthetic sorbents with enhanced properties for high-temperature CO_2-capture. Energy Procedia 4:1184–1191
21. Moradi G, Mohadesi M, Hojabri Z (2014) Biodiesel production by CaO/SiO_2 catalyst synthesized by the sol–gel process. Reac Kinet Mech Cat 113:169–186
22. Abanades JC, Anthony JE, Lu DY, Salvador C, Alvarez D (2004) Capture of CO_2 from combustion gases in a fluidized bed of CaO. AIChE J 20:1614–1622
23. Lenggoro IW, Itoh Y, Iida N, Okuyama K (2003) Control of size and morphology in NiO particles prepared by a low-pressure spray pyrolysis. Mater Res Bull 38:1819–1827
24. Cho YB, Seo G, Chang DR (2009) Transesterification of tributyrin with methanol over calcium oxide catalysts prepared from various precursors. Fuel Process Technol 90:1252–1258
25. Zhang X, Zhang Q, Tsubaki N, Tan Y, Han Y (2015) Carbon dioxide reforming of methane over Ni nanoparticles incorporated into mesoporous amorphous ZrO_2 matrix. Fuel 147:243–252
26. Luo MF, Zhong YJ, Yuan XX, Zheng XM (1997) TPR and TPD studies of CuO/CeO_2 catalysts for low temperature CO oxidation. Appl Catal A 162:121–131
27. Kang M, Song MW, Lee ChH (2003) Catalytic carbon monoxide oxidation over CoO_x/CeO_2 composite catalysts. Appl Catal A 251:143–156
28. Sayle TXT, Parker SC, Catlow RA (1992) Surface oxygen vacancy formation on CeO_2 and its role in the oxidation of carbon monoxide. J Chem Soc, Chem Commun 14:977–978
29. Tang X, Zhang B, Li Y, Xu Y, Xin Q, Shen W (2004) Carbon monoxide oxidation over CuO/CeO_2 catalysts. Catal Today 93–95:191–198

30. Cao JL, Wang Y, Yu XL, Wang SR, Wu SH, Yuan ZY (2008) Mesoporous CuO-Fe_2O_3 composite catalysts for low-temperature carbon monoxide oxidation. Appl Catal B 79:26–34
31. Ross RH (2012) Heterogeneous catalysis, fundamentals and applications. Elsevier, Barcelona
32. Kadossov E, Burghaus U (2008) Adsorption kinetics and dynamics of CO, NO and CO_2 on reduced CaO (100). J Phys Chem C 112:7390–7400
33. Wang M, Wang H, Zhao N, Wei W, Sun Y (2006) Synthesis of dimethyl carbonate from urea and methanol over solid base catalysts. Catal Commun 7:6–10
34. Li Q, Zhang W, Zhao N, Wei W, Sun Y (2006) Synthesis of cyclic carbonates from urea and diols over metal oxides. Catal Today 115:11–116
35. Sakuma K, Miyajima K, Mafuné F (2013) Oxidation of CO by nickel oxide clusters revealed by post heating. J Phys Chem A 117:3260–3265